On the modeling of narrow gaps using the standard boundary element method

Vicente Cutanda[a)]
Brüel & Kjær Sound & Vibration, Skodsborgvej 307, DK-2850 Nærum, Denmark

Peter Møller Juhl[b)]
ITF Institute of Applied Physics, Odense University/The Engineering College of Odense,
Niels Bohrs Allé 1, DK-5230 Odense M, Denmark

Finn Jacobsen[c)]
Department of Acoustic Technology, Technical University of Denmark, Ørsteds Plads,
Building 352, DK-2800 Kgs. Lyngby, Denmark

Numerical methods based on the Helmholtz integral equation are well suited for solving acoustic scattering and diffraction problems at relatively low frequencies. However, it is well known that the standard method becomes degenerate if the objects that disturb the sound field are very thin. This paper makes use of a standard axisymmetric Helmholtz integral equation formulation and its boundary element method (BEM) implementation to study the behavior of the method on two test cases: a thin rigid disk of variable thickness and two rigid cylinders separated by a gap of variable width. Both problems give rise to the same kind of degeneracy in the method, and modified formulations have been proposed to overcome this difficulty. However, such techniques are better suited for the so-called thin-body problem than for the reciprocal narrow-gap problem, and only the first is usually dealt with in the literature. A simple integration technique that can extend the range of thicknesses/widths tractable by the otherwise unmodified standard formulation is presented and tested. This technique is valid for both cases. The modeling of acoustic transducers like sound intensity probes and condenser microphones has motivated this work, although the proposed technique has a wider range of applications. © *2001 Acoustical Society of America.*
[DOI: 10.1121/1.1350399]

I. INTRODUCTION

Phenomena where the physical setup contains very close domain boundaries are not uncommon in practice. Typical cases are fins or appendages from bulky structures, thin plates, and shells. All of them have parts that are very thin compared to the overall dimensions. It is well known that the conventional boundary element method has difficulties in dealing with such tasks. Considerable effort has been put into this so-called thin-body problem in recent years in order to make it tractable with BEM, and different formulations have been proposed that can alleviate or remove such difficulties.[1–4]

There is a second family of cases that shares many features with thin bodies. This may be named the narrow-gap problem. Examples are coatings, lubricant layers, cracks, and some acoustic transducers. The domain of interest in these cases is situated *between* the close boundaries, and very often a two-dimensional simplification cannot be used if the transversal variations are of physical relevance.

BEM formulations that can deal effectively with thin bodies become of no use in narrow gaps, and only a few techniques remain that can provide results in practical engineering work. One of these techniques is described in this paper, which has been motivated by numerical modeling of sound intensity probes and condenser microphones.[5] The behavior of sound fields inside narrow gaps plays a central role in these devices. Therefore, the performance of BEM formulations in such situations must be understood in order to obtain meaningful results.

The conventional BEM has two difficulties whenever two parts of the surface are very close.[4] First, the coefficient matrix becomes ill-conditioned as the distance gets smaller, and second, the integrals are near singular and difficult to solve numerically. The methods proposed to get around these difficulties in the thin-body variant fall into two groups: multidomain methods and normal-derivative equation methods. In multidomain methods an imaginary surface is constructed so as to replace the original problem of a thin body in a single domain with bulky bodies in two domains or more, coupled at an imaginary surface.[2] Such methods are advantageous for certain problems such as muffler analysis, but for other cases the imaginary surface may be quite large and will therefore give rise to considerable computational work. The alternative methods involve the normal derivative of the Helmholtz integral equation (HIE). A popular implementation is a combination of the HIE with its normal derivative, since this combination also can be shown to overcome the nonuniqueness problem of the standard HIE.[6] A strategy often chosen is to apply the combined equation on the midsurface of the thin body.[1,3] Another procedure, which does not

---

[a)]Electronic mail: vcutanda@bksv.com
[b)]Electronic mail: pmjuhl@itf.sdu.dk
[c)]Electronic mail: fjac@oersted.dtu.dk

assume the approximation of an infinitely thin body, applies the HIE on one side of the thin body and its normal derivative on the other.[4]

For a plane narrow gap a multidomain strategy could be used in which the gap could be modeled as a two-dimensional problem coupled to an exterior three-dimensional problem. However, this approach is only approximate for any finite gap width, and not suitable for problems where the sound field details inside the gap are important. As to the combined formulation in Ref. 4, the regularizing effect seems to rely on a medium being present outside, as in the case of inclusions.

Since complete removal of the ill-conditioning in the gap case is problematic, it is interesting to examine whether the conventional formulation can still provide correct results for practical cases under such circumstances. As pointed out in Ref. 4, adequate treatment of the near-singular integrals can prevent a breakdown due to poor integration, but it leaves the ill-conditioning. We will show in this paper how a simple numerical integration strategy can extend the range of aspect ratios (smaller dimension/overall dimension) by several orders of magnitude despite ill-conditioning, thus placing most practical gap problems within reach of the standard BEM. Besides, the proposed numerical integration only requires a very small increase of computing resources.

The nature of the problem of close boundaries is reviewed in the next section, with emphasis on the features of the gap case. An explanation of the numerical integration technique developed follows. The remainder of the paper is dedicated to thin-body and narrow-gap test cases. An axisymmetrical formulation is used, which is outlined along with details of the study methodology. The behavior of the method's convergence towards the solution is analyzed on the test cases, as well as the ill-conditioning of the coefficient matrix. The influence of frequency, mesh density, and aspect ratio is investigated.

II. THE PROBLEM OF CLOSE DOMAIN BOUNDARIES

A. The standard Helmholtz integral equation (HIE)

The BEM approach to acoustic radiation and scattering problems is based on the Helmholtz integral equation that relates the pressure $p(Q)$ and normal velocity $\nu(Q)$ on the surface of a body of any shape (see Fig. 1) with the pressure at any point $p(P)$ and the pressure of an incoming wave $p^I(P)$.[7] The harmonic time dependence $e^{i\omega t}$ is omitted, giving

$$C(P)p(P)=\int_S\left(\frac{\partial G}{\partial n}p(Q)+ikz_0\nu(Q)G\right)dS+4\pi p^I(P),$$
(1)

where S is the surface of the body, Q a point on that surface, and P any exterior or interior point. The normal vector n is directed into the computational domain. The Green's function for 3D free space is
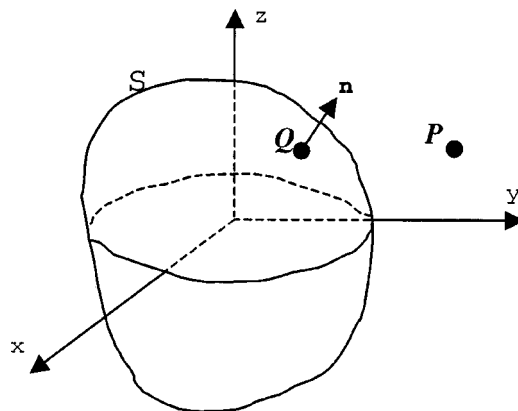
$$G(R)=\frac{e^{-ikR}}{R},\quad R=|P-Q|.$$
(2)

FIG. 1. Generic integration domain and boundary surface.

The factor $C(P)$ is the geometrical constant and represents the exterior solid angle at P. It is calculated by

$$C(P)=4\pi+\int_S\frac{\partial}{\partial n}\left(\frac{1}{R}\right)dS.$$
(3)

The expression (3) is valid for exterior problems; for interior problems 4π should be subtracted. In the present study only scattering by rigid bodies is considered; thus, $p^I(P)$ is the excitation and $\nu(Q)=0$, making Eq. (1) simpler. However, the coefficient matrix obtained from the BEM numerical implementation of (1) will be the same as for radiation problems, and therefore the conclusions discussed below will still be general. The standard collocation formulation will be used.

B. The thin-body problem

The case of a thin planar body has been discussed extensively in the literature, and hence the results are merely listed. For a thin disk using constant elements and unmodified numerical integration, the coefficient matrix of the BEM becomes

$$2\pi\begin{pmatrix}\mathbf{I} & \sim\!\mathbf{0}\\ \sim\!\mathbf{0} & \mathbf{I}\end{pmatrix},$$
(4)

where $\mathbf{I}$ is the identity matrix and $\sim\!\mathbf{0}$ is approximately a matrix of zeros. This matrix is perfectly conditioned, but does not lead to the correct solution of the problem.[8] The problem is grounded in the nonhandling of the near singularity of the integral as the integration point Q to the surface S_+ passes the collocation point P on the near surface S (see Fig. 2). With proper treatment of the near singularity, one finds a correct matrix representation for the problem[4,8]

$$2\pi\begin{pmatrix}\mathbf{I} & \sim\!\mathbf{I}\\ \sim\!\mathbf{I} & \mathbf{I}\end{pmatrix}.$$
(5)

Here, the near degeneracy is reflected in an ill-conditioned matrix, which potentially may lead to incorrect solutions. As mentioned in the Introduction, two solutions have been proposed to deal with thin bodies, the multidomain method and the use of the normal derivative. Both of them reformulate the problem in a way that makes the ill-conditioning disappear, although in the case of some combined formulations
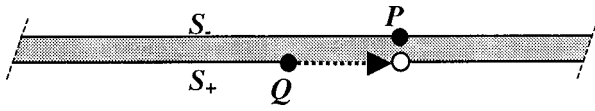
FIG. 2. Thin-body setup.

using the normal derivative, near-singular integrals are still present and must be taken care of.[4,9]

C. The narrow-gap problem

Consider a rigid bulky object with a narrow gap, as represented in Fig. 3. The surface on the exterior of the object is denoted by S, and the surfaces in the gap by S_- and S_+, respectively. Since there is no pressure jump across the gap in the limit of a gap of zero thickness, the normal derivative methods do not pose any new information for this kind of problems. The standard HIE for a scattering problem with such an object is

$$C(P)p(P) = \int_S p(Q)\frac{\partial G}{\partial n}dS + \int_{S_-} p_-(Q)\frac{\partial G}{\partial n}dS$$

$$+ \int_{S_+} p_+(Q)\frac{\partial G}{\partial n}dS + 4\pi p^I(P). \quad (6)$$

Let P be on S. In the limit of an infinitely narrow gap, continuity of the pressure requires that $p_- = p_+$ so the two integrals for the two gap surfaces cancel out. Hence, in the limit of narrow gaps the sound field outside the gap is not influenced by the sound field inside the gap. This is in agreement with what one would expect physically. Therefore, the solution strategy for a problem involving a very narrow planar gap with rigid surfaces could be to solve an exterior problem neglecting the gap, and then to solve the gap problem as a two-dimensional interior problem with the pressures obtained for the exterior problem as the boundary conditions. However, if the gap width cannot be neglected, if parts of the gap surface are of finite impedance, and/or if viscosity is to be taken into account, the need for a simultaneous analysis of the gap and the exterior field is envisaged. If the near singularity is properly taken into account, the block of identity matrices of Eq. (5) is found in the matrix equivalent of Eq. (6)

$$\begin{pmatrix} \mathbf{A} & \mathbf{D} & -\mathbf{D} \\ \mathbf{C} & 2\pi\mathbf{I} & \sim 2\pi\mathbf{I} \\ \sim\mathbf{C} & \sim 2\pi\mathbf{I} & 2\pi\mathbf{I} \end{pmatrix} \begin{pmatrix} p \\ p_- \\ p_+ \end{pmatrix} = 4\pi p^I. \quad (7)$$

The first block of rows in Eq. (7) refers to collocation points on the exterior surface S, and the second and third block of rows refer to collocation points on S_- and S_+, respectively. Again, the near degeneracy due to the two close surfaces is reflected in ill-conditioning of the coefficient matrix. If the near singularity is not dealt with properly, the lower right corner of the coefficient matrix is to be replaced with Eq. (4)

$$\begin{pmatrix} \mathbf{A} & \mathbf{D} & -\mathbf{D} \\ \mathbf{C} & 2\pi\mathbf{I} & \sim \mathbf{0} \\ \sim\mathbf{C} & \sim \mathbf{0} & 2\pi\mathbf{I} \end{pmatrix} \begin{pmatrix} p \\ p_- \\ p_+ \end{pmatrix} = 4\pi p^I, \quad (8)$$
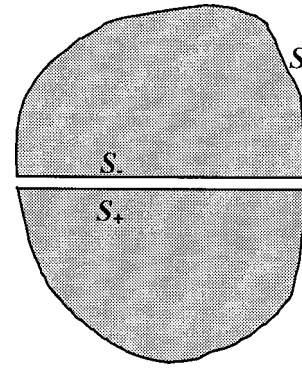

FIG. 3. Narrow-gap setup.

and the resulting (false) system of equations will be well-conditioned. In the latter case, which represents a standard numerical implementation, it is easy to show that the solution will tend towards zero inside the gap as the gap width tends towards zero. The solution outside the gap will still tend towards the solution of the equivalent exterior problem with the gap removed.

III. IMPROVEMENT OF THE NUMERICAL INTEGRATION

To achieve the goal of obtaining valid solutions for narrow-gap problems, the strategy chosen is the improvement of the numerical integration technique. A system of equations of the form in (7) should be guaranteed for a range of aspect ratios of practical importance. As mentioned in the last section, there is still ill conditioning, and therefore the accuracy of the elements in the coefficient matrix, which are obtained by numerical integration, imposes a limit to the aspect ratio that can be calculated. Nevertheless, if this limit is high enough, the cases left out will be too narrow to have practical use or even physical meaning.

Several authors propose ways to handle near-singular integrals. For example, in Refs. 4 and 9 an analytical removal of the near singularity that splits the integral is performed. The resulting terms are treated with variable changes and the Stokes theorem in order to reduce or eliminate their difficulty. However, the approach taken in this paper will be numerical, not analytical.

The behavior of a near-singular integrand differs in many ways from a genuine singularity. If a collocation point is in the neighborhood of an element to be integrated, it produces a perturbation on the integrand around its projection on the element, more localized and more acute the shorter the distance. This effect can be observed in Fig. 4, which is a near-singular integrand along a one-dimensional element. It has been obtained from the disk test case to be presented in the following section. Note that integrand values are represented in a logarithmic scale and that only a part of the element is shown. It becomes clear from Fig. 4 why standard numerical integration methods, like Gauss–Legendre, miss this troublesome area for a given relative distance and lead to results as shown in Eqs. (4) and (8). This situation has often been described as the ''breakdown'' of the BEM standard formulation.
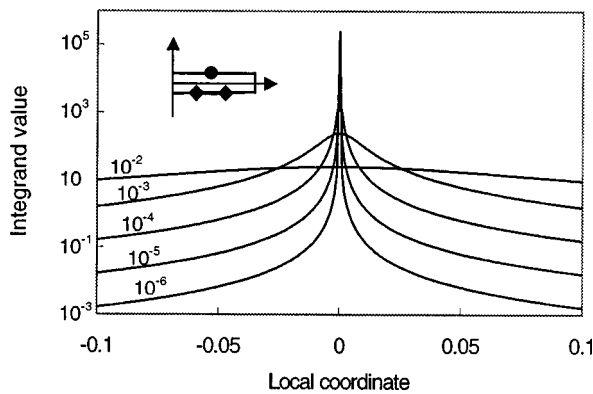
FIG. 4. Near-singular behavior of an integrand in the thin disk calculation. Abscissas are local coordinates along the element $[-1,1]$; ordinates are values of the integrand on a logarithmic scale. The curves are integrands with a collocation point at 10^{-2}, 10^{-3}, 10^{-4}, 10^{-5}, and 10^{-6} units' distance from the local coordinate 0. The disk radius is 1 unit. Five elements per disk side are used.

Only very limited improvement is obtained by merely increasing the order of the numerical integration formula. The integration does not concentrate the effort around the near singularity, where the integrand has a peak. The use of numerical formulas designed for singular integrals has also been considered, but they do not perform well due to the different nature of the near-singular integrand.

Another possible choice is an adaptive numerical integration routine. Such routines have been used for many years on all kinds of problems and are implemented in most mathematical software packages. Basically, the algorithm tries to decrease the integration error down to a given value. To do this, the error is estimated during every iterative step, and more integration points are used on the difficult areas. When applied to near-singular integrals in BEM, there is a clear improvement. However, these methods often fail in the limit of very close collocation points. The floating-point precision of the machine is reached during the internal calculation of integration error estimates, with unpredictable results. This lack of reliability and control on the routine behavior seems to rule them out.

An optimal numerical integration scheme for this particular problem should be simple enough to minimize errors but, on the other hand, it should concentrate the effort around the difficult area. If the information about the near singularity and its strength can be used in order to perform each integration in the most appropriate way, the computer load can also be reduced.

In view of this, the approach finally adopted employs an exponential interval division according to the expected near-singular behavior, as shown in Fig. 5. In this study, one-
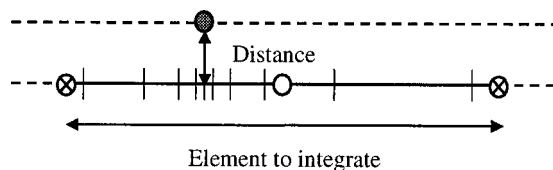

FIG. 5. Exponential interval division on a one-dimensional quadratic element. Relative distance and local coordinate of the collocation point are used to calculate the number and sizes of the subintervals.

TABLE I. Processing time results on a DEC Alpha 433 MHz for the two-cylinder test case (see Sec. IV B) with 60 elements. Gauss–Legendre numerical integration of order 20 and the interval division technique are compared.

Gap width	Integration	Time (s)	Result
10^{-2}	Gauss	82.7	Good
	Division	91.4	Good
10^{-3}	Gauss	83.0	Fail
	Division	93.2	Good
10^{-4}	Gauss	83.2	Fail
	Division	93.9	Good
10^{-5}	Gauss	82.7	Fail
	Division	94.4	Good
10^{-6}	Gauss	82.6	Fail
	Division	96.7	Fail

dimensional quadratic elements are used, but the technique can be translated to other implementations. The distance from each subinterval boundary to the collocation point projection is expressed by $c \cdot b^n \cdot d$, where b and c are constants, d is the distance from collocation point to the element, relative to the element size, and n is the subinterval number. In practical calculations, it was adjusted to $b=2$ and $c=2^{-5}$. Each subinterval can be numerically integrated using low-order standard techniques. In this way the information available about the integrand is used to perform the numerical integration, and no complex adaptive integration strategy is needed.

The improved integration does not involve a significant increase in computer load. Computational effort is only applied where it is necessary; that is, only in those cases where the collocation point is very close to the element and, within that element, around the near singularity and proportional to its strength. Table I presents some run times for the narrow-gap test case and a 60-element fixed mesh. The interval division technique adds around 10%–20% to the normal processing time, with a slight increase for narrower gaps. This is logical if we consider that the technique is only used to calculate an order of N elements in an $N \times N$ matrix.

IV. TEST CASES

A. BEM axisymmetrical formulation

If an axisymmetric body or bodies on the same axis are considered, it is possible to simplify the standard BEM from a surface integral to an integral along the generator and another over the angle of revolution, in a cylindrical coordinate system. The use of a cosine expansion of $p(Q)$ and $\nu(Q)$ in orthogonal terms allows the isolation of the singularities contained in the revolution integrals so that only the generator has to be discretized, saving computing time and storage capacity. Although the excitations described in this paper are also axisymmetrical, the cosine expansions permit nonaxisymmetrical boundary conditions. This implementation retains most features of the full 3D version, which means that the problem of close boundaries can be studied more easily and over a larger number of test cases.[10]
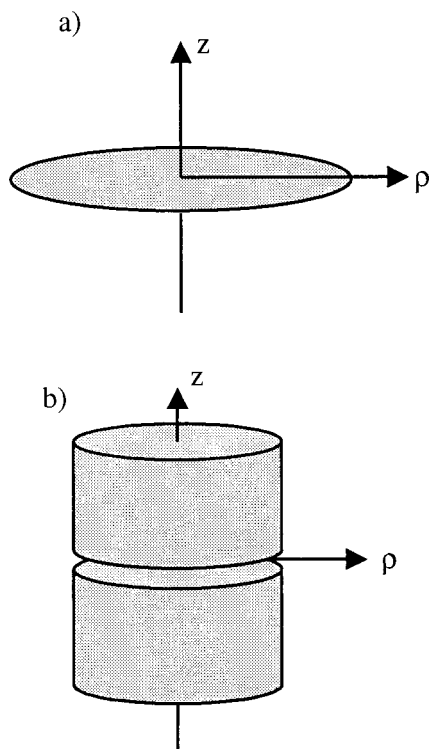
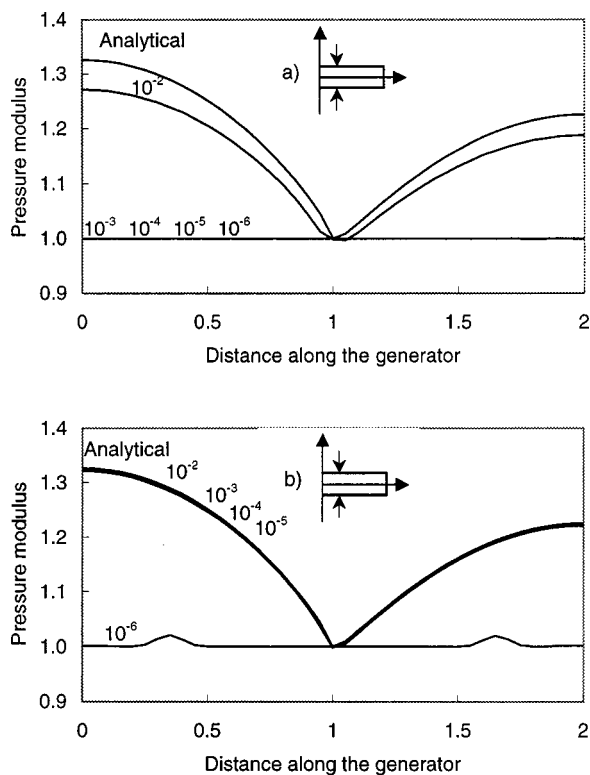FIG. 6. Test cases. (a) thin disc; (b) narrow gap.

FIG. 7. Calculated sound-pressure modulus on the generator of a disk [see Fig. 6(a)] of variable thickness using a mesh of 10 elements per unit, 20 elements in total. The thicknesses are 10^{-2}, 10^{-3}, 10^{-4}, 10^{-5}, and 10^{-6}. The analytical solution for a infinitely thin disk is also plotted. An axial plane wave of $ka=1$ and unit amplitude is scattered by the disk. Calculations using (a) Gauss–Legendre numerical integration of order 20; (b) with interval division as explained in Sec. III.
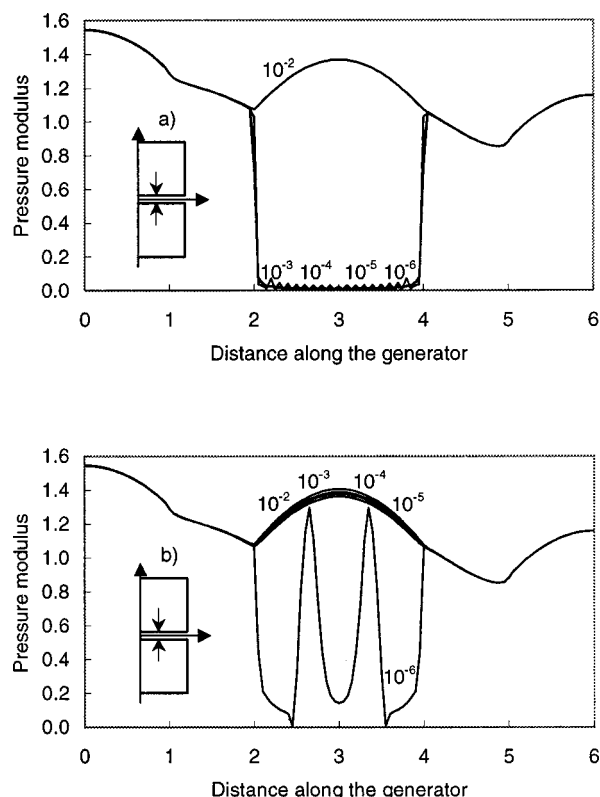

FIG. 8. Calculated sound-pressure modulus on the generator of two coaxial rigid cylinders [see Fig. 6(b)] separated by a variable narrow gap calculated using a mesh of 10 elements per unit, 60 elements in total. The gap widths are 10^{-2}, 10^{-3}, 10^{-4}, 10^{-5}, and 10^{-6}. An axial plane wave of $ka=1$ and unit amplitude is scattered by the setup. Calculations using (a) Gauss–Legendre numerical integration of order 20; (b) with interval division as explained in Sec. III.

B. Test cases

Two test cases have been chosen to represent the thin-body problem and the narrow-gap problem. These are, respectively, a disk of variable thickness and two cylinders with a common axis that form a narrow gap. They are represented in Fig. 6.

These cases have rotational symmetry along the cylindrical coordinate θ and therefore the axisymmetrical BEM formulation can be applied. The bodies are supposed to be rigid (infinite impedance) and excited by a plane wave coming from the z^+-axis direction. Several values of ka (wave number times radius) have been used in the calculations, but only the results for $ka=1$ are presented, since no relevant variation with the frequency has been observed. The radius a of disk and cylinders is normalized to 1, as well as cylinder lengths.

The numerical implementation is made by dividing the generators into line elements. Both pressure and geometry are modeled using quadratic shape functions.

C. Sound-pressure results

The sound-pressure modulus along the generator of the objects in Fig. 6 is shown in Figs. 7 (disk) and 8 (gap) for a variety of thicknesses/widths. Standard Gauss–Legendre integration [Figs. 7(a)/8(a)] succeeds only if the disks or gaps are thicker than 10^{-2} units, while the proposed interval di-

vision can give good results down to 10^{-5} units [Figs. 7(b)/8(b)]. The two breakdowns are different. An integration failure causes the pressure to drop to zero on the close surfaces, while the improved integration avoids this down to a point where ill-conditioning is too serious for the limited precision of the computer to cope with, and unpredictable results appear. Other calculations not shown here have demonstrated that neither mesh density nor frequency has any influence on the ill-conditioning breakdown. It is only dependent on the aspect ratio.

Figure 7 also includes the corresponding analytical solution for a disk of zero thickness, which can be obtained as a series of oblate spheroidal functions. This solution has been calculated in order to validate the results and study the convergence. A brief summary is given in the Appendix of this paper.

The pressure increase in the gap observed in Fig. 8 can be explained in the limiting case of a vanishing gap. Ideally, the external sound field would not be influenced by the pres-

ence of a very narrow gap. Therefore, considering the gap as two-dimensional, the sound pressure along the radius (generator) inside the gap has the form of a Bessel function.[11] Its boundary condition is the sound pressure on the external surface connected to the gap (abscissas 2 and 4 in Fig. 8). For $ka = 1$, there are no zeros of the Bessel function within the gap; therefore, only a pressure increase is observed.

D. Convergence of the improved solution

Using the calculated complex sound pressure on the generator nodes and the corresponding analytical values for an infinitely thin disk, it is possible to study the convergence of the thin-disk calculation as a function of mesh density and disk thickness.

The thicknesses examined are small enough to make them physically very similar to a disk with no thickness. The error is calculated as the length of the residual vector relative to the analytical solution

$$\text{Relative error} = \frac{\sqrt{\Sigma_{j=1}^{M}[(\text{Re}(P_{j\ \text{analytical}}) - \text{Re}(P_{j\ \text{calculated}}))^2 + (\text{Im}(P_{j\ \text{analytical}}) - \text{Im}(P_{j\ \text{calculated}}))^2]}}{\sqrt{\Sigma_{j=1}^{M}[\text{Re}(P_{j\ \text{analytical}})^2 + \text{Im}(P_{j\ \text{analytical}})^2]}}, \tag{9}$$

where $P_{j\ \text{analytical}}$ is the analytical solution at node j and $P_{j\ \text{calculated}}$ is the calculated complex pressure at the same node. M is the total number of nodes of every solution. See Fig. 9.

Unfortunately, the narrow-gap case does not have a suitable analytical solution. The two-dimensional analogy mentioned in the last section is not precise enough to study convergence, since it is dependent on the boundary conditions at the rim that are themselves subject to calculation errors, which are aggravated because of the sharp edge singularity.[12] The convergence can nevertheless be studied by using a solution with a very fine mesh as a reference. This is what Fig. 10 represents.

The convergence is clear in the disk case, and independent of the thickness. Only the 10^{-6} case cannot converge

due to the ill-conditioning of the coefficient matrix, but thicker disks do not show any strange behavior. The gap case is physically more complicated because what happens inside the gap is strongly influenced by the phenomena on the gap rim; therefore, the convergence pattern differs. Nevertheless, the solutions clearly converge again except for the 10^{-6} case. The use of a calculated solution as a reference produces also a shift in the error scale.

E. Ill-conditioning

The condition number of the coefficient matrix has been calculated for a number of mesh densities and disk/gap thicknesses. It was shown in Sec. III that a good numerical integration in a problem of close surfaces produces an ill-
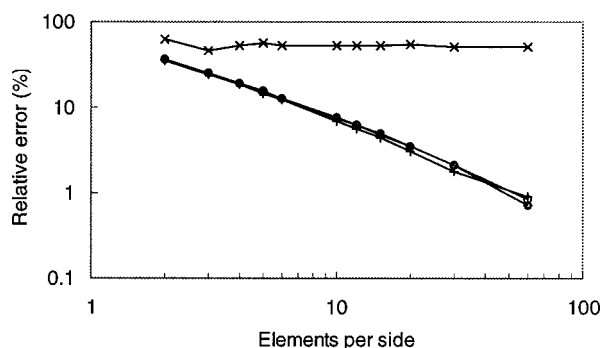

FIG. 9. Convergence towards the analytical solution of a thin disk [see Fig. 6(a)] of variable thickness, using the proposed numerical integration. The thicknesses are 10^{-2} (+), 10^{-3} ($\diamond$), 10^{-4} ($\square$), 10^{-5} ($\bigcirc$), and 10^{-6} ($\times$). The relative error is represented as a function of the mesh density. An axial plane wave of $ka = 1$ and unit amplitude is scattered by the disk.
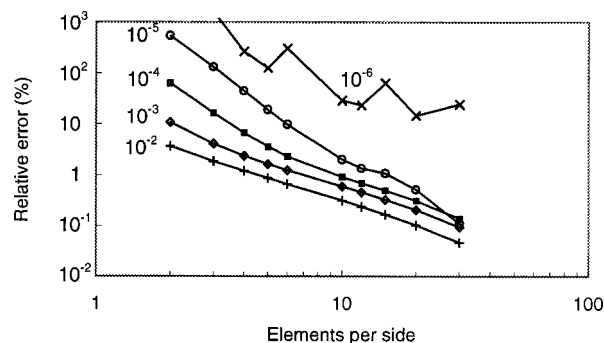

FIG. 10. Convergence towards the ''true'' solution of a narrow gap [see Fig. 6(b)] of variable width, using the proposed numerical integration. The widths are 10^{-2} (+), 10^{-3} ($\diamond$), 10^{-4} ($\square$), 10^{-5} ($\bigcirc$), and 10^{-6} ($\times$). The relative error in the gap nodes is represented as a function of the mesh density. An axial plane wave of $ka = 1$ and unit amplitude is scattered by the cylinders.
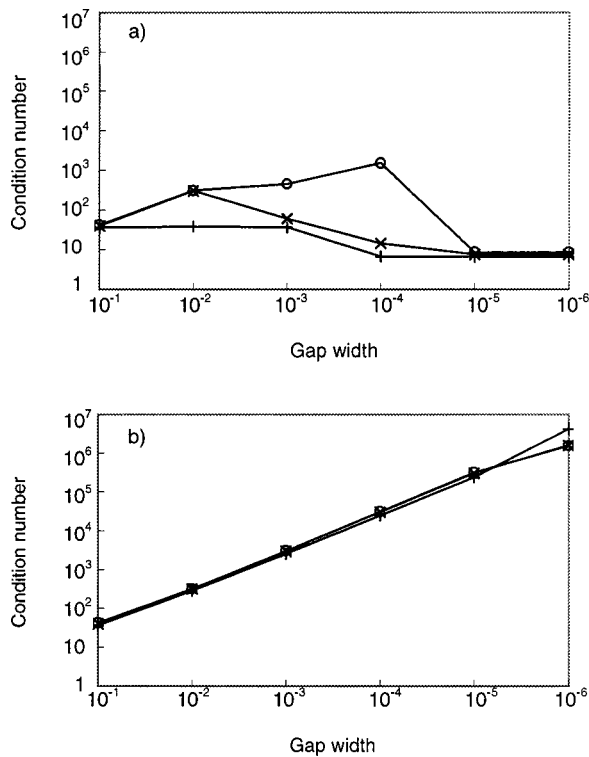
FIG. 11. Condition number of the coefficient matrix for the narrow-gap test case, as a function of gap width. Three mesh densities are plotted: 2 (+), 10 (×), and 60 (○) elements per unit. Calculations using (a) Gauss–Legendre numerical integration of order 20; (b) with interval division as explained in Sec. III. Calculation made with $ka = 1$.
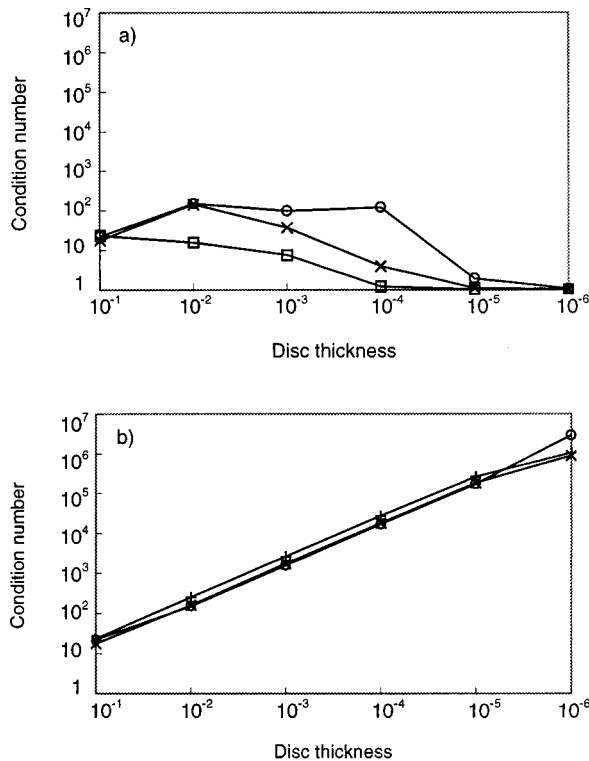

FIG. 12. Condition number of the coefficient matrix for the thin-disk test case, as a function of thickness. Three mesh densities are plotted: 2 (+), 10 (×), and 60 (○) elements per side. Calculations using (a) Gauss–Legendre numerical integration of order 20; (b) with interval division as explained in Sec. III. Calculation made with $ka = 1$.

conditioned system of equations, and therefore a high condition number of the coefficient matrix. Conversely, a failure of the integration generates low condition numbers, but with erroneous solutions.

Figures 11 and 12 show that the ill-conditioning behaves similarly in the two test cases. If the near-singular integrals are not dealt with, the condition number does not grow very much, but the calculation gives erroneous results. When the interval division technique is used the condition number grows exponentially as the surfaces get closer, no matter which mesh density is used. The frequency also has very little influence, as other calculations not presented here have shown. Hence, the aspect ratio indeed seems to determine the condition number, independently of whether we deal with narrow gaps or thin bodies.

V. CONCLUSIONS

It has been shown that a case of practical importance in engineering like the narrow gap can be modeled using conventional BEM despite the ill-conditioning of the coefficient matrix and with no need of denser meshes. A convergence study has also revealed that the solution improves normally for gradually denser meshes. A simple strategy of interval division with low computational cost is enough to extend the range of tractable aspect ratios by three orders of magnitude, from 10^{-2} to 10^{-5}. This makes it possible to deal with problems like condenser microphones and sound intensity probes, which have motivated this study. For example, the air layer behind the diaphragm of a 1/2-in. condenser microphone is about 20 μm, giving an aspect ratio of about 10^{-3}.

APPENDIX: ANALYTICAL SOLUTION FOR SCATTERING BY A FLAT DISK

The infinitely thin disk is the limiting case of the oblate spheroid, which is better described in the oblate spheroidal coordinate system (ξ, η, ϕ). Its relation with rectangular Cartesian coordinates is

$$x = \tfrac{1}{2}d\sqrt{(\xi^2+1)(1-\eta^2)}\cos\phi,$$
$$y = \tfrac{1}{2}d\sqrt{(\xi^2+1)(1-\eta^2)}\sin\phi, \quad z = \tfrac{1}{2}d\xi\mu. \tag{A1}$$

The wave equation is separable in this coordinate system into spheroidal wave functions, thus providing analytical solutions for a range of cases. The particular solution used in this paper corresponds to an infinitely thin hard disk ($\xi = 0$ and d = diameter) excited by a plane wave coming from the positive z axis. The sound pressure (incident and scattered) on its surface can be expressed by the series[13]

$$P^i + P^s = \frac{2}{ka}\sum_{n=0}^{\infty}\frac{i^n}{N_{0n}(-ika)}\frac{S_{0n}(-ika,-1)S_{0n}(-ika,\eta)}{R_{0n}^{(3)'}(-ika,i0)},$$
$$\tag{A2}$$

where S_{mn} are the oblate spheroidal angular functions, $R_{mn}^{(3)}$ are the derivatives of the oblate spheroidal radial functions of the third kind, and N_{nm} are the normalization factors.[14] These functions are also expressed as infinite series, and computer algorithms have been used to calculate them with sufficient accuracy.[15]

[1] R. Martinez, ''The thin-shape breakdown (TSB) of the Helmholtz integral equation,'' J. Acoust. Soc. Am. **90**, 2728–2738 (1991).

[2] C. Y. R. Cheng, A. F. Seybert, and T. W. Wu, ''A multidomain boundary element solution for silencer and muffler performance prediction,'' J. Sound Vib. **151**, 119–129 (1991).

[3] T. W. Wu and G. C. Wan, ''Numerical modeling of acoustic radiation and scattering from thin bodies using a Cauchy principal integral equation,'' J. Acoust. Soc. Am. **92**, 2900–2906 (1992).

[4] G. Krishnasamy, F. J. Rizzo, and Y. Liu, ''Boundary integral equations for thin bodies,'' Int. J. Numer. Methods Eng. **37**, 107–121 (1994).

[5] F. Jacobsen, V. Cutanda, and P. M. Juhl, ''A numerical and experimental investigation of the performance of sound intensity probes at high frequencies,'' J. Acoust. Soc. Am. **103**, 953–961 (1998).

[6] A. J. Burton and G. F. Miller, ''The application of integral equation methods to the numerical solutions of some exterior boundary value problems,'' Proc. R. Soc. London, Ser. A **323**, 201–210 (1971).

[7] A. F. Seybert, B. Soenarko, F. J. Rizzo, and D. J. Shippy, ''An advanced computational method for radiation and scattering of acoustic waves in three dimensions,'' J. Acoust. Soc. Am. **77**, 362–368 (1985).

[8] T. W. Wu, ''A direct boundary element method for acoustic radiation and scattering from mixed regular and thin bodies,'' J. Acoust. Soc. Am. **97**, 84–91 (1995).

[9] Y. Liu and F. J. Rizzo, ''Scattering of elastic waves from thin shapes in three dimensions using the composite boundary integral equation formulation,'' J. Acoust. Soc. Am. **102**, 926–932 (1997).

[10] P. M. Juhl, ''An axisymmetric integral equation formulation for free space nonaxisymmetric radiation and scattering of a known incident wave,'' J. Sound Vib. **163**, 397–406 (1993).

[11] P. M. Morse, *Vibration and Sound*, 2nd ed. (The Acoustical Society of America, New York, 1983).

[12] P. M. Juhl, ''A note on the convergence of the direct collocation boundary element method,'' J. Sound Vib. **212**, 703–719 (1998).

[13] J. J. Bowman, T. B. A. Senior, and P. L. E. Uslenghi, *Electromagnetic and Acoustic Scattering by Simple Shapes* (North-Holland, Amsterdam, 1969).

[14] C. Flammer, *Spheroidal Wave Functions* (Stanford University Press, Stanford, 1957).

[15] S. Zhang and J. Jin, *Computation of Special Functions* (Wiley, New York, 1996).